Accepted Manuscript

Hydrogen production by tailoring the brookite and Cu_2O ratio of sol-gel Cu-TiO_2 photocatalysts

Mariana Hinojosa Reyes, Roberto Camposeco-Solís, Rodolfo Zanella, Vicente Rodríguez González

PII: S0045-6535(17)30969-4

DOI: 10.1016/j.chemosphere.2017.06.066

Reference: CHEM 19460

To appear in: *ECSN*

Received Date: 23 November 2016

Revised Date: 10 May 2017

Accepted Date: 15 June 2017

Please cite this article as: Hinojosa Reyes, M., Camposeco-Solís, R., Zanella, R., Rodríguez González, V., Hydrogen production by tailoring the brookite and Cu_2O ratio of sol-gel Cu-TiO_2 photocatalysts, *Chemosphere* (2017), doi: 10.1016/j.chemosphere.2017.06.066.

Hydrogen production by tailoring the brookite and Cu_2O ratio of sol-gel Cu-TiO_2 photocatalysts

Mariana Hinojosa Reyes[a]*, Roberto Camposeco-Solís[b], Rodolfo Zanella[c], Vicente Rodríguez González[b]

[a]Facultad de Ciencias, Universidad Autónoma de San Luis Potosí, San Luis Potosí, S.L.P., 78000, México, México.

[b]División de Materiales Avanzados, IPICYT, Instituto Potosino de Investigación Científica y Tecnológica, Camino a la Presa San José 2055 Col. Lomas 4a. sección C.P. 78216, San Luis Potosí, S.L.P., México.

[c]Centro de Ciencias Aplicadas y Desarrollo Tecnológico, Universidad Nacional Autónoma de México, Circuito Exterior S/N, Ciudad Universitaria, A. P. 70-186, Delegación Coyoacán, C.P. 04510, México D. F. México.

e-mail: kittyhinojosa@hotmail.com

Abstract

Cu-TiO_2 photocatalysts were prepared by the sol-gel method. Copper loadings from, 1.0 to 5.0 wt. % were used. The materials were annealed at different temperatures (from 400 to 600 °C) to study the formation of brookite and copper ionic species. The photocatalysts were characterized by X-ray diffraction, UV-vis, Raman and XPS spectroscopies, H_2-temperature programmed reduction (TPR), N_2 physisorption, and SEM–EDS to quantify the actual copper loadings and characterize morphology. The photocatalysts were evaluated during the hydrogen photocatalytic production using an ethanolic solution (50 % v/v) under UV and visible radiation. The best hydrogen production was performed by Ti-Cu 1.0 with

an overall hydrogen production that was five times higher than that obtained with photolysis. This sample had an optimal thermal treatment at 500 °C, and at this temperature, the Cu_2O and brookite/anatase ratio boosted the photocatalytic production of hydrogen. In addition, a deactivation test was carried out for the most active sample (TiO_2-Cu 1.0), showing unchanged H_2 production for three cycles with negligible Cu lixiviation. The activity of hydrogen-through-copper production reported in this research work is comparable with the one featured by noble metals and that reported in the literature for doped TiO_2 materials.

Keywords

Cu-TiO_2, Water Splitting, Cu_2O, Anatase – Brookite Ratio, Copper lixiviation, Cyclic H_2 Production.

1. Introduction

Due to the lifestyle in modern societies, fossil fuels have become an important energy source due to the use of motorized vehicles, which burn tons of fuels causing high levels of atmospheric pollution (Dincer, 2000). From this perspective, the humankind needs new types of environmentally friendly energy sources with no toxic wastes, low costs, and mainly that can be obtained from renewable sources such as water.

The Fujishima and Honda (Fujishima and Honda, 1972) water splitting discovery using a TiO_2 photoelectrode has been modified and applied ever since in many kinds of scavenger solutions to enhance hydrogen production by this photocatalytic method.

The TiO_2 semiconductor in the anatase crystalline phase has a conduction band that is more positive than the redox potential of O_2/H_2O (1.23 V), i.e., the necessary energy to carry out the water splitting, which is 1.23 eV ($H_2O_{(l)} \rightarrow H_{2(g)} + 1/2O_{2(g)}$). It is important to mention that the TiO_2 rutile crystalline phase does not have this optical property due to the position of the conduction band energy (Kudo and Miseki, 2009). Moreover, although there are reports on brookite-anatase mixtures that have shown higher photocatalytic activities than those displayed by the single TiO_2 anatase phase or anatase/rutile mixture, there are only few reports on the tailoring of the brookite/anatase ratio in TiO_2 mixtures using a controlled synthetic method (Tay et al., 2013). Brookite also has a conduction band that is more positive than the redox potential of water (Kudo and Miseki, 2009), but TiO_2 anatase presents the disadvantage of electron-hole pair recombination during the H_2 photocatalytic process. To avoid this problem, the introduction of surface or structural defects through the insertion of noble or transition metals has been proposed since low Fermi levels of noble metals provide electron transfers from TiO_2 to the loaded noble metal (Xu et al., 2010), resulting in a more efficient separation of charge carriers, thus enhancing the potential of hydrogen generation. Moreover, the doping of TiO_2 creates defect states such as surface oxygen vacancies in the semiconductor.

Several reports have shown that the surface functionalization of TiO_2 with nanoparticles of precious metals such as gold, platinum or palladium, etc. (Ni et al., 2007) has displayed high hydrogen photocatalytic production, however, these elements are expensive and, in some cases, scarce. An alternative to avoid the high cost of using noble metals is the selection of other low cost metals such as copper (Choi and Kang, 2007). Specifically, Cu_2O is a simple metal oxide semiconductor with low band gap energy. As shown in an

energy correlation between the band gap model of Cu_2O and the redox potentials of relevant electrode reactions in an aqueous solution at pH 7, the conduction and valence band edges of Cu_2O, which are separated by band gap energies from 2.0 to 2.2 eV, seem to be available for the reduction and oxidation of water, respectively (Hara et al., 1998).

In this manuscript, the use of Cu-TiO_2 catalysts in the photocatalytic production of hydrogen is studied. Some new insights regarding the use of the sol-gel method to dope TiO_2 with copper ions and its effects on the crystallite and brookite/anatase ratio tailored by different calcination temperatures, is discussed. The enhancement of the water hydrogen photocatalytic production was achieved with the optimal anatase/brookite ratio in presence of Cu^{1+}/Cu^{2+} ions without apparent lixiviation of copper ions.

2. Experimental section

2.1. Sol – gel TiO_2 synthesis

Sol-gel-TiO_2-Cu photocatalysts were prepared by means of a controlled sol-gel process using titanium (IV) isopropoxide (Sigma-Aldrich, 97%) as titanium precursor and copper nitrate trihydrate (II) (Sigma-Aldrich, 98%) as copper precursor (doping agent); ethanol (Le Cap Group, 96%) and distilled water were used as solvents. According to a reported sol-gel synthesis (Hinojosa et al., 2012), an appropriate amount of nitrate salt was dissolved in water to obtain 1.0, 2.5, and 5.0 wt. % of copper. The TiO_2-Cu catalysts were prepared by adding 75.6 mL of titanium isopropoxide dropwise to a 22.9-mL ethanol/18-mL water solution to which the copper precursor solution was added into a 4-neck-round-bottom flask (1 L) equipped with magnetic stirrer and thermometer. The alkoxide/ethanol/water molar ratio was 1/3/8. Later on, the solution was stirred vigorously at 50°C during the addition of

the reagents. Subsequently to this step, the solution was gradually heated up to 70 °C. The gelled product was aged for 48 h at 70°C. The solvents and unreacted precursors were slowly removed at 80 °C and dried overnight under vacuum at 100 °C. Finally, the materials were thermally treated at different temperatures in an interval ranging from 400 to 600 °C for 4 h at a rate of 2 °C min^{-1}. The samples were identified as Ti-Cu X, where X represents the copper load (wt. %).

2.2. Characterization techniques

The thermally treated samples were characterized by X-ray diffraction in order to identify crystalline phases using an X-ray diffractometer SmartLab RIGAKU with CuKα radiation (1.5404 Å); the crystalline phases were corroborated with Raman spectroscopy, using a Micro-Raman Renishaw spectrometer equipped with a He-Ne laser (633 nm).

Diffuse reflectance UV–vis spectra of the photocatalysts were obtained using a Cary 5000 (UV-vis-NIR) spectrophotometer; spectralon teflon (from Agilent) was used as a reference blank and the band gap energy was determined by using the Kubelka-Munk method. The physical adsorption of N_2 at -196 °C was carried out using a Quantachrome Autosorb 1 automatic instrument on previously out-gassed samples at 150 °C. The Brunauer-Emmett-Teller method (BET method) was used to calculate the specific surface area. Temperature programmed reduction was performed in a ChemBET TPR/TPD chemisorption analyzer by Quantachrome Instruments within a temperature interval ranging from room temperature to 600 °C with a rate of 10 °C/min and flow of 30 mL min^{-1} of H_2 (10%) / Ar (gas). An energy dispersive X-ray spectroscopy (EDS) detector (ESEM FEI-QUANTA 200) was used for the

semiquantitative determination of copper content in the photocatalysts. SEM images were obtained by Dual Beam FIB/SEM: FEI Helios Nanolab 600i.

XPS was performed with an XPS, Multiab 2000 system with an X-ray AlKα (1486.6 eV) source operated at 15 KV and 1 mA, 400W and 1 ma. The binding energy was determined by using carbon C (1 s) as reference line (284.6 eV). Peak fitting was done by using the XPS fitting program XPSPEAK 41 with Shirley background.

2.3. Water splitting test

The photocatalytic activity of the Ti-Cu materials was evaluated in a home-made cylindrical glass reactor with an inner quartz tube equipped with a UV pen ray Hg lamp (λ = 254 nm, I_0 = 4400 microwatts/cm^2) and visible radiation Kr lamp (λ = 450 nm). This glass reactor had a full operation volume of 250 mL and the scavenger solution consisted of water-ethanol (100:100 mL, 50 vol. % of H_2O), where ethanol was purchased from Le Cap Group (96%). In all the experiments, 50 mg of photocatalyst powder were used and the suspension was stirred for 20 minutes while it was purged with nitrogen to remove the dissolved oxygen from the solution. After oxygen was removed, the reactor system was sealed and the UV lamp was turned on. Hydrogen determination was done every hour for 8 h in a gas chromatograph by Thermo Scientific with thermal conductivity detector and packed column by Thermo Scientific TracePLOT TG-BOND Msieve 5A. The system was calibrated previously in order to quantify the hydrogen production.

Once the reaction finished, the photocatalysts were recovered and dried at 80 °C for 8 h and then analyzed by X-ray diffraction to elucidate the possible structural changes in the materials.

For the stability test, three cycles of 8 h each were carried out for the selected most active photocatalyst (Ti-Cu 1.0), which was calcined at 500 °C. After running the experiments, the UV lamp was turned off, the produced hydrogen was released and the reaction system was purged with nitrogen until the hydrogen chromatographic signal was zero. Afterwards, the reactor system was sealed, after 8 h, and the lamp was turned on again to start the next cycle and so on until the third cycle was completed.

Finally, the copper lixiviation in the Ti-Cu 1 sample was determined for a period of 24 h of water splitting reaction from the final solution by inductively coupled plasma optical emission spectroscopy (ICP-OES) using a 730-ES spectrometer from Varian Inc.

3. Results and discussion

3.1. Characterization of Materials

3.1.1. X-ray diffraction

Figure 1 shows the diffractogram patterns of the Ti-Cu samples. Independently of the copper loading, the presence of the anatase crystalline phase (JCPDS 21-1272) was detected. The brookite crystalline phase (JCPDS 29-1360) was also detected and grew along with the increase in copper load in TiO_2, see Figure 1a. Diffraction peaks related to copper presence are shown in Figure 1b. At around 36 and 42º, two peaks related to the crystallographic planes of Cu_2O were detected (JCPDS 05-0667), (111) and (200), respectively. At around 40º, a crystallographic plane, (111), related to the growth of CuO was detected (JCPDS 45-0937).

The XRD patterns for the Ti-Cu 1.0 sample calcined at temperatures ranging from 400 to 500°C are shown in Figure 1c. Again, the anatase crystalline phase prevails with the

presence of low intensity peaks related to the brookite crystalline phase at temperatures below 500 °C. Figure 1d shows the temperature effect on the evolution of copper oxides. At temperatures up to 550 ºC, the (200) plane corresponding to Cu_2O disappears, while the (111) plane related to CuO is evidently visible. Therefore, at low calcination temperatures, the formation of Cu_2O is favored while at higher temperatures, the formation of CuO is promoted.

Additionally, at low calcination temperatures, the peak width of the (101) plane is wider, which indicates the formation of fine brookite crystallites. However, with the increasing calcination temperatures, the intensity of the (101) plane increases and becomes narrower, which is due to the growth of crystallites (Yu et al., 2003). Despite high calcination temperatures, it is important to mention that the rutile crystalline phase is not present, which is due to the fact that copper restricts the growth of anatase and shifts to higher temperatures its transformation to rutile (Bokhimi et al., 1997).

3.1.2. Effect of annealing temperature and copper loading

An additional study to elucidate the brookite/anatase ratio was done using the following equation (Zhang and Banfield, 2000):

$$W_B = \frac{k_B A_B}{k_A A_A + A_R + k_R A_R}$$

Where the k_A and k_B coefficients have values of 0.886 and 2.721, respectively, and W_B represents the brookite/anatase crystalline phase ratio. A_A represents the intensity of the

anatase (101) peak and A_B the intensity of brookite (121) peak (Zhang and Banfield, 2000). In Table 1, the brookite percentage and its corresponding crystallite size are shown.

According to the data presented in Table 1, it is observed that the brookite percentage increases with the copper content, therefore, the Ti-Cu 1.0 photocatalyst has the lowest brookite percentage (8.92 %) and the Ti-Cu 5.0 sample has the highest one (13.31 %).The crystallite size of the photocatalysts was determined using the Scherrer equation; likewise for the anatase crystalline phase and the different copper contents, see Table 1. The crystallite size also correlates with the percentage of brookite with sizes around 13.0 and 17.5 nm, respectively. Therefore, the copper concentration has a direct relationship with the brookite growth, restricting, on the other hand, the anatase crystallite growth. As for the calcination temperatures, the higher the calcination temperature, the lower the brookite percentage, which passed from 17.55 % for the sample treated at 400 °C to 0.00 % for the sample treated at 600 °C. The opposite case occurs for the crystallite sizes: the lower the brookite percentage, the bigger the crystallite size, Table 1.

The average size is around 17 nm, except for the Ti-Cu 2.5 photocatalyst with a size of 20 nm. For the case of the Ti-Cu 1.0 sample calcined at different temperatures, the crystallite size ranged from 8 to 40 nm: the higher the calcination temperature, the higher the crystallite size, Table 3. The temperature increase caused the crystallites to grow since they gain more energy than the growth activation energy (Zhang et al., 2000).

3.1.3. Raman spectroscopy

Raman spectra of the photocatalysts are shown in Figure 2. With this technique, the presence of anatase as main crystalline phase was corroborated; in Figure 2a-b, the vibrational Raman modes for anatase are not labeled, which occur at 396, 515 and 638 cm^{-1} and are assigned to B_{1g}, $A_g + B_{1g}$ and E_g, respectively (Ohsaka et al., 1978) and also to the presence of the brookite crystalline phase. In the same figure, two strong vibrational modes related to brookite are shown, assigned and labeled as B_{1g} and B_{2g}, which occurred at 320 and 366 cm^{-1}, respectively (Tompsett et al., 1995).

With the help of the main vibrational mode (E_g) that occurred at 144 cm^{-1}, evidence of the possible Cu doped TiO_2 was found. Figure 2c shows the Eg vibrational mode of the Ti-Cu photocatalyst with different copper contents, where the position of this band is at around 143.4 cm^{-1} in all the cases with a full width at half maximum (FWMH) from 10 to 11 cm^{-1}, Table 2.

In the case of the copper photocatalysts calcined at different temperatures, Figure 2d, a wide variation in the FWHM is observed; the band position is modified from 142.3, 142.8, 143.4, and 144.6 to 145 cm^{-1} for 400, 450, 500, 550, and 600 °C, respectively, Table 3. This shift toward high wavenumbers is related to the structure modification as a function of the calcination temperature and brookite/anatase ratio, which is due firstly to a shortening and/or rigidity of the Ti-O bond of this E_g vibrational mode caused by the increase in surface oxygen vacancies formed by the incorporation of Cu^{2+} into the TiO_2 lattice, which reduces the O/Ti rate (Zhu et al., 2007). Due to this incorporation, the FWHM is also disturbed, where at a higher calcination temperature, a smaller FWHM is obtained. Phonon confinement and non-stoichiometry effects are responsible for the blueshift and broadening of the lowest-frequency E_g Raman mode (Yu et al., 2003). The non-stoichiometry is due to

the creation of surface oxygen vacancies produced by the Cu^{2+} incorporation into the TiO_2 lattice.

3.1.4. XPS analysis

The XPS analysis was carried out to determine the chemical and electronic structure of copper in the Ti-Cu photocatalysts. Figure 3 shows a representative peak-fit of the Cu $2p_{3/2}$ core level and its corresponding shake-up satellites. Satellite peaks characteristic of Cu^{2+} photocatalysts are found at around 945 and 962.5 eV, see supplementary information S1, which can be seen as the dominant peaks in Ti-Cu 5.0 (500°C). In particular, the peak-fit for the Ti-Cu 5.0 (500°C) sample exhibited the largest core shake-up satellites with respect to the Ti-Cu 1.0 (500°C), Ti-Cu 1.0 (550°C) and Ti-Cu 1.0 (600°C) samples, indicating a clear surface oxidation process for Cu during the annealing process. Deconvolution line shapes using a Shirley background were used to fit peaks, where the Cu^{+1} state was found at 932 eV and the Cu^{+2} state was located at 933 eV. The used curve-fitting parameters are in agreement with those reported by Chusuei et al., 1999, and Huang et al., 2009. The ratio of the sum of the areas of the deconvoluted peaks was used to estimate the amount of Cu^{+2} transformed into Cu^{+1} by the Ti-Cu samples. The XPS results confirmed the Cu^{+1} and Cu^{+2} oxidation states of copper present on the Ti-Cu surface. This result was also supported by XRD and other studies reported elsewhere (Huang et al., 2009, Sinatra et al., 2015). According to the annealing temperature increments, the Cu^{+}/Cu^{2+} rate decreased, see intensities in Figure 3. Also, when the copper content was increased, this rate was strongly affected, diminishing notably. Therefore, at low copper contents (1wt.%) and calcination temperature of 500 ºC, the formation of Cu_2O on the TiO_2 surface is guaranteed. The

shake-up satellite, which was ascribed to the open shell structure $3d^9$ L (L is for ligand), led to multiple splitting of Cu^+ in Cu $2p_{3/2}$ at 935 eV and $2p_{1/2}$ at 955 eV (Perry and Taylor, 2006, Borgohain et al., 2002, Ghijsen et al., 1988, Chen et al., 2012, Sinatra et al., 2015). On the other hand, the contribution of Cu^{2+} was increased by the annealing temperature, which also increased the metal loading on TiO_2.

3.1.5. UV-vis spectroscopy

The band gap energy (Eg) of each photocatalyst is shown in Table 1. Bare TiO_2 has an Eg of 3.4 eV, Ti-Cu 1.0 of 3.3 eV, Ti-Cu 2.5 of 3.2eV, and finally Ti-Cu 5.0 of 2.3 eV, Table 2. The reduction of the Eg value was closely related to the increase in the copper content in TiO_2 due to the creation of trap levels between the conduction and valence bands of TiO_2 (Nagaveni et al., 2004).

The Ti-Cu 1.0 photocatalyst, calcined at different temperatures, showed no evident changes in the Eg values (3.2 and 3.3 eV). Although CuO and Cu_2O absorb in the visible region due to Eg values of 1.2 and 2.0 eV (Yu et al., 2007), respectively. The formation of copper oxides is negligible due to the high TiO_2 content; therefore, TiO_2 could mask the low band gap of the copper oxides, not showing any shift toward the visible region due to the temperature effect.

With this spectroscopic technique, it can be assumed that copper incorporation exerts a surface effect on the modified TiO_2, the band gap energy, and apparently, the calcination temperature, and therefore, the brookite/anatase ratio does not play a specific role in this optical property. Figure 1S shows the UV-vis spectra of the Ti-Cu photocatalysts and

changes can be observed when copper loadings are increased or at different calcination temperatures.

3.1.6. Temperature programmed reduction

The temperature programmed reduction thermograms are shown in Figure 4. Figure 4a shows the effect of the variation of the copper loading; for copper loadings of 1.0 wt. %, a low intensity peak with a width from 180 to 250 °C is visible. This peak is associated with the $Cu^{2+} \rightarrow Cu^{+}$ reduction, which is related to the copper oxide, CuO, $Cu^{2+} \rightarrow Cu^{1+}$ reduction (Kundakovic and Stephanopoulos, 1998, Fierro et al., 1996). In addition, the Ti-Cu 2.5 and Ti-Cu 5.0 samples show a well-defined reduction peak that starts at 160 and ends at 210 °C; this peak is also related to the $Cu^{2+} \rightarrow Cu^{+}$ reduction. The shoulders observed for the Ti-Cu 5.0 sample at 225 and 275 °C are associated with the continuous reduction of Cu^{+} to Cu^{0} species (Beutel et al., 1996).

The behavior of the Ti-Cu 1 photocatalyst calcined at temperatures between 400 and 600 °C is shown in Figure 4b. The calcination temperatures of 500, 550, and 600 °C reveal a well-defined reduction peak associated with the Cu^{2+} ion reduction centered at 195.8 °C (Chen et al., 2012, Nagaveni et al., 2004, Li et al., 2008) while at calcination temperatures of 400 and 450 °C, lower intensity peaks at temperatures between 280 and 450 °C with maximal intensities at 340 and 400 °C are observed; these peaks may be associated with the $Cu^{+} \rightarrow Cu^{0}$ reduction, but shifted to higher temperatures with respect to the other samples. This shift is associated with well-dispersed copper into the TiO_2 lattice. According to the literature, the copper reduction goes as follows $CuO \rightarrow Cu_2O \rightarrow Cu^{0}$ (Kim et al., 2003).

It is important to mention that either Cu^{2+} or Cu^{+} species are slightly detected by XRD due to the low copper concentration, but they were well detected by the TPR technique and well corroborated the Cu^{+}/Cu^{2+} ratio by XPS spectroscopy.

For the Ti-Cu 1.0, Ti-Cu 2.5 and Ti-Cu 5.0 samples, three reduction peaks were observed, which were ascribed to the reduction of CuO and Cu_2O species on TiO_2 (Guangjun et al., 2011). The peaks observed at 183.7, 202.8 and 221.8 were attributed to the reduction of CuO. Likewise, the little shoulder observed at 279 °C in the Ti-Cu 5.0 sample was assigned to the reduction of crystalline CuO (Wan et al., 2008). Finally, Figures 4a and 4b show that as the copper load is increased and the annealed temperature is enhanced, a shift towards lower temperatures leading to the formation of Cu^{2+} species occurs, which is in agreement with the results observed by XPS.

3.1.7. N_2 adsorption-desorption

With the help of the nitrogen adsorption-desorption technique, the surface area of the photocatalysts was corroborated, and the BET areas are reported in Tables 2 and 3 for the different copper contents and different annealing temperatures, respectively. In the case of different copper contents, at higher concentrations, a lower surface area is observed. The sol-gel TiO_2 has values of 64.6, 1.0 wt. %, 59.5, 2.5 wt. %, 40.0, and 5.0 wt. % of 35.2 m^2/g, Table 2. As for the different-annealing-temperature photocatalysts, the higher the calcination temperature, the lower the surface area, starting at 115.3 m^2/g for 400 °C, and ending with a surface area of 14.0 for the catalyst treated at 600 °C, Table 3.

According to the isotherms presented in Figure 5, a type IV isotherm was obtained for the materials, which is representative of mesoporous solids such as titania due to a high P/Po

ratio (Choi et al., 2004). Regarding the types of hysteresis loops, the H2 type represents the hysteresis generated by the Ti-Cu 0.0, Ti-Cu 1.0, and Ti-Cu 1.0 samples treated at 400, 450, and 550 °C; this kind of loops is representative of narrow necks, and wide bodies such as ink-bottle pores. In the case of the Ti-Cu 2.5 and Ti-Cu 5.0 samples, the representative hysteresis loops are of the H4 type, which is associated with narrow, slit-like pores; finally, the Ti-Cu 1-0 treated at 600 °C presents H3 hysteresis loops, which are characteristic of slit-like pores (Sing et al., 1985).

An additional analysis was carried out to calculate the normalized surface area, NS_{BET}, according to the following equation (Vradman et al., 2005):

$$NS_{BET} = (S_{BET\ of\ catalysts}) / (1-x)*(S_{BET\ of\ support}).$$

where NS_{BET} is the normalized surface area, $S_{BET\ of\ catalysts}$ is the surface area of the catalysts, X is the weight fraction of copper loading, and $S_{BET\ of\ support}$ is the surface area of the catalysts.

The results are shown in Tables 2 and 3. The normalized surface area data suggest that a value close to 1 indicates that the copper introduction caused minimal reduction in the surface area, thus insignificant reduction in the normalized surface area. These effects are observed in Ti-Cu 1.0 annealed at 400, 450, and 500 °C with values of 0.95, 0.94 and 0.93, respectively. On the other hand, the normalized surface area was affected when the metal loading was increased to 2.5 and 5.0 wt.%; likewise, when the annealing temperature was 600°C, the normalized surface area was decreased notably.

3.1.8. Semiquantitave chemical composition, EDS

The semiquantitative determination of the chemical composition of copper in the photocatalysts was carried out by the SEM–EDS technique. The results of the Cu composition are presented in Table 2. The EDS analyses show that the mean atomic percentages of copper were quite similar to the nominal values. The semiquantitative copper loadings were 1.01, 2.49, and 4.63 wt. % for the Ti-Cu 1.0, Ti-Cu 2.5, and Ti-Cu 5.0 samples, respectively. The EDS spectra taken from different regions of the same sample indicate that the Ti-Cu nanopowders were obtained with controlled copper doping concentrations and uniform copper ion distributions. In Figure 2S, the typical morphology of TiO_2 can be seen, which corresponds to agglomerates of spherical nanoparticles, which independently of the copper loadings preserve the same morphology.

The XPS results confirmed the existence of Cu_2O, and the Raman spectroscopy confirmed the presence of Cu^{2+} doping the TiO_2 framework, producing surface oxygen vacancies that can favor the photocatalytic process.

3.1.9. Hydrogen production test

The previously characterized materials were evaluated in the hydrogen photocatalytic production. Figure 6 shows the results for the Ti-Cu materials with different copper loadings (from 0 to 5 wt. %), and calcined at 500 °C. Each curve corresponds to the hydrogen production rate for 8 h of reaction test and after the subtraction of the hydrogen production obtained by water photolysis. According to these results, the optimal copper loading is 1.0 wt. % with a H_2 production of 3865 $\mu mol\ g^{-1}h^{-1}$; this quantity corresponds to four times more H_2 production with respect to photolysis. For copper contents of 2.5 and

5.0 wt. %, lower hydrogen production rates of 2290 and 2856 µmol $g^{-1}h^{-1}$ were obtained, respectively. It is important to mention that bare TiO_2 presents a very low hydrogen production of 963 µmol $g^{-1}h^{-1}$, just above the hydrogen production obtained by the water-ethanol photolysis, which means that even with a low copper loading, the hydrogen production was enhanced remarkably due to the copper incorporation into the TiO_2 lattice. As for the induction period for the samples treated at 500 ºC, see Figure 6ab, Ti-Cu 1.0 continued having the highest rate of hydrogen production (99 µmol h^{-1}); the Ti-Cu 2.5 and Ti-Cu 5.0 samples showed a similar rate of 50 µmol h^{-1} while the poorest sample, the bare TiO_2, featured a rate of 32 µmol h^{-1}. It is important to mention that the Ti-Cu 0.0 sample showed negligible activity because of the rapid recombination of conduction band electrons and valence band holes and as a result of the absence of $H^{\cdot}$ recombination centers for hydrogen evolution (Majeed et al., 2016).

In addition, copper incorporation creates an optimal brookite/anatase ratio since brookite and mainly the Cu_2O formation lead to the photocatalytic production of hydrogen because Cu_2O is a semiconductor with small band gap energy. Cu_2O shows an energy correlation between the band gap and the redox potentials of relevant electrode reactions in an aqueous solution. The conduction and valence band edges of Cu_2O, which are separated by band gap energies from 2.0 to 2.2 eV, seem to be adequate for easing the reduction and oxidation of water, respectively (Hara et al., 1998, Li et al., 2015). Thus, maybe a *pn*-junction could be achieved due to the combination of Cu_2O and an n-type semiconductor, TiO_2, which results in higher photocatalytitc activity due to the presence of an electrostatic field at the junction, faciliting the charge separation between electrons and holes (Sarkar et al., 2013, Wang et al., 2010, Shifu et al., 2009). Some authors explain this situation with help of

photoluminescence spectroscopy (Yang et al., 2010). Other authors explain the pn-heterojunction according to the induction of oxidation process of organic pollutants (Bessekhouad et al., 2005).

Figure 6a-b shows the hydrogen production obtained when the fresh Ti-Cu 1.0 sample was annealed at different temperatures: 400, 450, 500, 550, and 600 °C. It is shown that the sample annealed at 500 °C has the highest hydrogen production with 3865 µmol $g^{-1}h^{-1}$, followed by the treatment at 550 °C with 2565 µmol $g^{-1}h^{-1}$; then, at 450 °C with 2118 µmol $g^{-1}h^{-1}$, and finally at 400 and 600 °C with a similar hydrogen production of 1600 µmol $g^{-1}h^{-1}$ (after 8 h). It is important to note that after annealing at 500 °C, copper is present as Cu_2O and CuO (Cu^+, and Cu^{2+} species, respectively), which provides a high delocalization of the electronic density, improving the redox reactions related to water splitting – hydrogen production; it also avoids the recombination of photogenerated holes and electrons due to the possible *pn*-heterojunction that could be carried out by TiO_2 and copper oxides.

According to the induction period, see Figure 6bb, the highest rate of hydrogen production in the first reaction hour was followed according to this trend: 550 > 500 > 450 > 600 > 400 ºC. However, once the reaction finished (8 h), the tendency changed to 500 > 550 > 450 > 600 = 400 ºC. The change in the tendency is attributable to the copper oxides. Just above 550 ºC, appeared the formation of CuO while at 500 ºC, the presence of Cu_2O prevails.

It is important to mention that there is an effective interfacial charge transfer in both species (Mondal et al., 2016). The Ti-Cu 1.0 – 500 °C sample has a 0.098 brookite/anatase ratio that enhances the hydrogen photocatalytic production or produces the highest hydrogen quantity due also to redox properties of the bookite phase; more specifically, due to the fact that its conduction band is more positive than the redox potential of the O_2/H_2O pair (Xu et

al., 2010). It has been reported that low brookite contents enhance dramatically the hydrogen photocatalytic production as seen here (Kandiel et al., 2010).

Another important phenomenon that could occur in the copper photocatalysts is the one related to work function, which means that the electron transfer is facilitated from a material with a lower work function to another with a higher work function value, acting this last material as an efficient trap for the photogenerated electrons, preventing the e^-/h^+ recombination, and as consequence, improving the photocatalytic activity. The work function values of TiO_2 (-3.90 eV) allow an efficient electron transfer from TiO_2 to CuO/Cu_2O (-4.35 eV) (Oros et al, 2014, Yang and Rhee, 2007). Maybe, the low copper loading in the TiO_2 photocatalysts could act as a co-catalyst, improving the hydrogen photocatalytic production, where the copper load exerts an effect increasing the surface area; therefore, larger particles exert a shadow effect which implies a larger transportation of electrons and cannot participate in the photochemical process; thus, this shadow effect reduces the catalyst activity, at least on a per unit mass basis (Saupe et al., 2005).

It is important to mention that the overall hydrogen produced by the copper photocatalysts is considerable with respect to other Pd, Pt or Au on TiO_2 photocatalysts analyzed under the same conditions with 5644, 2317, and 6242 µmol $g^{-1}h^{-1}$ (Hinojosa et al., 2016) with respect to 2958 µmol $g^{-1}h^{-1}$ of the Ti-Cu samples analyzed here. The two first values were obtained by our group and have not yet been published. Therefore, the results reported in the present work give an indication of the possibility of preparing new materials that are cheaper than noble-metal-based catalysts, which represents 124-time-higher savings with the use of copper catalysts with regard to gold catalysts.

According to the copper loading and calcination temperature optimization, the Ti-Cu 1.0 sample annealed at 500 °C was submitted to a stability test using the same ethanolic solution. After three cycles of reaction, no deactivation of the photocatalysts was observed, and similar hydrogen production was produced after each cycle, around 4000 µmol $g^{-1}h^{-1}$ in each cycle, Figure 6c. This result is a key issue for practical application.

Due to the band-gap of the copper materials, the TiO_2 with different copper contents were evaluated during the water splitting reaction under visible radiation, see Figure 7. In this case, the effect exerted by the copper incorporation during the H_2 evolution is obviously remarkable. The bare TiO_2 shows no hydrogen production, while the rest of the samples show H_2 production of 437, 400, and 345 µmol $g^{-1}h^{-1}$ for the Ti-Cu 1.0, 2.5, and 5.0 samples, respectively. Therefore, the copper incorporation at different loadings diminished the band gap energy, which allowed the photocatalytic hydrogen production under visible light, where the values are above those reported in the literature for doped TiO_2 materials (Dholam et al., 2009, Kato and Kudo, 2002, Khan et al., 2008).

To corroborate the copper stability into the TiO_2 materials during the photocatalytic experiments, the materials were recovered after the reaction and characterized by X-ray diffraction. After reaction, the materials maintained the same structural conformation, and also the copper oxides did not show any alteration after being irradiated, see Figure 8.

To confirm the structural stability of copper in the TiO_2 lattice, the reaction solution was analyzed by ICP and an overall copper lixiviation of 0.036 mg L^{-1} after the 24-h-reaction test was observed. This last information corroborates the structural stability of the photocatalyst, indicating that copper is strongly bound to the TiO_2 lattice, where this value is 70 times lower than the initial copper concentration of 2.5 mg L^{-1}, which corresponds to

the 1 wt.% of 50 mg of photocatalyst dissolved in 200 mL of ethanolic solution. It is important to mention that TiO_2-Cu materials have already been used in a similar reaction, but high lixiviation of copper during the water splitting process has been reported (Kudo and Miseki, 2009).

Finally, in Figure 9, according to normalized surface areas and the photocatalytic activity, the following graphs were done. Here, it is evident that with the lowest copper content (doping agent), the highest H_2 production was achieved, and also at 500 °C, we also had the highest H_2 production, which corresponds to the minimal/optimal annealing temperature. Optimal conditions for the synthesized materials were 1 wt.% of doping agent and annealing temperature at 500 °C for this kind of catalyst.

4. Conclusions

In this work, an alternative Cu/TiO_2 photocatalyst for hydrogen production by the water splitting reaction is presented. The advantages of copper doping during the gelling step are high activity, negligible copper lixiviation after several reaction cycles and lower cost of this catalyst in comparison with expensive novel metallic Pt, Pd or Au TiO_2 photocatalysts. The high stability and hydrogen production of the Ti-Cu 1.0 material annealed at 500 °C (2957.6 µmol $g^{-1}h^{-1}$) was due to several aspects: i) a higher formation of Cu_2O than CuO. Cu_2O has a band gap energy that is similar to that of the redox potential, which is available for the reduction and oxidation of water, ii) optimal copper loading that led to an optimal brookite ratio into the TiO_2 anatase crystalline phase, iii) copper performance to avoid the e^-/h^+ recombination and promote the charge transfer to enhance the redox reaction in the

water splitting reaction for hydrogen production, which is related to the work functions of both TiO_2 and Cu^+.

Finally, these kinds of Cu/TiO_2 photocatalysts are good candidates to be used under visible radiation due to a decrease in the band gap energy when the copper loading is incorporated into the framework in the photocatalysts.

Acknowledgements

The authors would like to thank DGAPA UNAM for supporting this work within the frame of the IN105416 project and CONACYT-CB-2011/169597, Infra-2014/225945 projects. We also thank the LINAN and LAMBAMA for the equipment and infrastructure provided. We wish to thank V. Maturano Rojas, B. A. Rivera Escoto, G. Labrada Delgado, Ma. Carmen Rocha Medina, and J. M. Martínez Andrade for their valuable support.

References

Dincer, I., 2000. Renewable energy and sustainable development: a crucial review. Renew. Sust. Energ. Rev. 4, 157 – 175.

Fujishima, A., Honda, K., 1972. Electrochemical photolysis of water at a semiconductor electrode. Nature. 238, 37 – 38.

Kudo, A., Miseki, Y., 2009. Heterogeneous photocatalyst materials for water splitting. Chem. Soc. Rev. 38, 253 – 278.

Tay, Q., Liu, X., Tang, Y., Jiang, Z., Sum, T. C., Chen, Z., 2013. Enhanced photocatalytic hydrogen production with synergistic two-phase anatase/brookite TiO_2 nanostructures. J. Phys. Chem. C. 117, 14973 – 14982.

Xu, S., Ng, J., Zhang, X., Bai, H., Sun, D. D., 2010. Fabrication and comparison of highly efficient Cu incorporated TiO_2 photocatalyst for hydrogen generation from water. Int. J. Hydrogen Energ. 35, 5254 – 5261.

Ni, M., Leung, M. K. H., Leung, D. Y. C., Sumathy, K., 2007. A review and recent developments in photocatalytic water-splitting using TiO_2 for hydrogen production. Renew. Sust. Energ. Rev. 11, 401 – 425.

Choi, H. J., Kang, M., 2007. Hydrogen production from methanol/water decomposition in a liquid photosystem using the anatase structure of Cu loaded TiO_2. Int. J. Hydrogen Energ. 32, 3841 – 3848.

Majeed, I., Nadeem, M. A., Hussain, E., Waterhouse, G. I. N., Badshah, A., Iqbal, A., Nadeem, M. A., Idriss, H., 2016. On the synergism between Cu and Ni for photocatalytic hydrogen production and their potential as substitutes of noble metals. Chem. Cat. Chem. 8, 3146 – 3155.

Hara, M., Kondo, T., 1998. Cu_2O as a photocatalyst for overall water splitting under visible light irradiation. Chem. Comm. 357 – 358.

Hinojosa-Reyes, M., Rodríguez-González, V., Arriaga, S., 2012. Enhancing ethylbenzene vapors degradation in a hybrid system based on photocatalytic oxidation UV/TiO_2-In and a biofiltration process. J. Hazard. Mater. 209-210 (2012) 365-371.

Yu, J-G., Yu, H-G., Cheng, B., Zhao, X-J., Yu, J. C., Ho, W-K., 2003. The effect of calcination temperature on the surface microstructure and phtocatalytic activity of TiO_2 thin films prepared by liquid phase deposition. J. Phys. Chem. B. 107, 13871 – 13879.

Bokhimi, X., Morales, A., Novaro, O., López, T., Chimal, O., Asomoza, M., Gómez, R., 1997. Effect of copper precursor on the stabilization of titania phases, and the optical properties of Cu/TiO2 prepared with the sol-gel technique. Chem. Mater. 9, 2616 – 2620.

Zhang, H., Banfield, J. F., 2000. Understanding polymorphic phase transformation behavior during growth of nanocrystalline aggregates: Insights from TiO_2. J. Phys. Chem. B. 104, 3481 – 3487.

Zhang, W. F., He, Y. L., Zhang, M. S., Yin, Z., Chen, Q., 2000. Raman scattering study on anatase TiO_2 nanocrystals. J. Phys. D. 33, 912 – 916.

Ohsaka, T., Izumi, F., Fujiki, Y., 1978. Raman spectrum of anatase, TiO_2. J. Raman Spectrosc. 7, 321 – 324.

Tompsett, G. A., Bowmaker, G. A., Cooney, R. P., Metson, J. B., Rodgers, K. A., Seakins, J. M., 1995. The Raman spectrum of brookite, TiO_2 (Pbca, Z = 8). J. Raman Spectrosc. 26, 57 – 62.

Zhu, J., Ren, J., Huo, Y., Bian, Z., Li, H., 2007. Nanocrystalline Fe/TiO_2 visible photocatalyst with a mesoporous structure prepared via a nonhydrolytic sol-gel route. J. Phys. Chem. C. 111, 18965 – 18969.

Chusuei, C.C., Brookshier, M.A., Goodman D.W., 1999. Correlation of relative X-ray photoelectron spectroscopy shake-up intensity with CuO particle size. Langmuir. 15, 2806–2808.

Huang. L., Peng. F., Ohuchi. F.S., 2009. “In situ” XPS study of band structures at Cu_2O/TiO_2 heterojunctions interface. Surf. Sci. 603. 2825–2834.

Perry, D. L., Taylor, J. A., 1986. X-ray photoelectron and Auger spectroscopic studies of Cu_2S and CuS. J. Mater. Sci. Lett. 5, 384 – 386.

Borgohain, K., Murase, N., Mahamuni, S., 2002. Synthesis and properties of Cu_2O quantum particles. J. Appl. Phys. 92, 1292 – 1297.

Ghijsen, J., Tjeng, L. H., van Elp, J., Westerink, E. J., Sawatzky, G. A., Czyzyk, M. T., 1988. Electronic structure of Cu_2O and CuO. Phys. Rev. B. 38, 11322 – 11330.

Chen, S., Zhang, H., Wu, L., Zhao, Y., Huang, C., Ge, M., Liu, Z., 2012. Controllable synthesis of supported Cu-M (M = Pt, Pd, Ru, Rh) bimetal nanocatalysts and their catalytic performances. J. Mater. Chem. 22, 9117 – 9122.

Sinatra, L., LaGrow, A. P., Peng, W., Kirmani, A. R., Amassian, A., Idriss, H., O. M., Bakr., 2015. A $Au/Cu_2O–TiO_2$ system for photo-catalytic hydrogen production. A pn-junction effect or a simple case of in situ reduction? J. Catal. 322 109-117.

Nagaveni, K., Hegde, M. S., Madras, G., 2004. Structure and photocatalytic activity of $Ti_{1-x}M_xO_{2\pm\delta}$ (M = W, V, Ce, Zr, Fe and Cu) synthesized by solution combustion method. J. Phys. Chem. B. 108, 20204 – 20212.

Yu, H., Yu, J., Liu, S., Mann, S., 2007. Template-free hydrothermal synthesis of CuO/Cu_2O composite hollow microspheres. Chem. Mater. 19, 4327 – 4334.

Kundakovic, L., Stephanopoulos, M. F., 1998. Reduction characteristics of copper oxide in cerium and zirconium oxide systems. Appl. Catal. A. 171, 13 – 29.

Fierro, G., Jacono, M. L., Inversi, M., Porta, P., Cioci, F., Lavecchia, R., 1996. Study of the reducibility of copper in CuO – ZnO catalysts by temperature-programmed reduction. Appl. Catal. A. 137, 327 – 348.

Beutel, T., Sárkány, J., Lei, G. D., Yan, J. Y., Sachtler, W. M. H., 1996. Redox chemistry of Cu/ZSM-5. J. Phys. Chem. 100, 845 – 851.

Li, G., Dimitrijevic, N. M., Chen, L., Rajh, T., Gray, K. A., 2008. Role of surface/interfacial Cu^{2+} sites in the photocatalytic activity of coupled $CuO\text{-}TiO_2$ nanocomposites. J. Phys. Chem. C. 112, 19040 – 19044.

Sarkar, D., Ghosh, C. K., Mukherjee, S., Chattopadhyay, K. K., 2013. Three dimensional Ag_2O/TiO_2 Type-II (p-n) nanoheterojunctions for superior photocatalytic activity. ACS Appl. Mater. Interfaces. 5, 331 – 337.

Wang, X., Liu, G., Lu, G. Q., Cheng, H-M., 2010. Stable photocatalytic hydrogen evolution from water over ZnO-CdS core-shell nanorods. Int. J. Hydrogen Energ. 35, 8199 – 8205.

Shifu, C., Sujuan, Z., Wei, L., Wei, Z., 2009. Study on the photocatalytic activity of p-n junction photocatalyst Cu_2O/TiO_2. J. Nanosci. Nanotechnol. 9, 4397 – 4403.

Yang, L., Luo, S., Li, Y., Xiao, Y., Kang, Q., Cai. Q. 2010. High efficient photocatalytic degradation of p-nitrophenol on a unique Cu_2O/TiO_2 p-n heterojunction network catalyst. Environ. Sci. Technol. 44, 7641 – 7646.

Bessekhouad, Y., Robert, D., Weber, J. V. 2005. Photocatalytic activity of Cu_2O/TiO_2, Bi_2O_3/TiO_2 and $ZnMn_2O_4/TiO_2$ heterojunctions. Catal. Today. 101, 315 – 321.

Kim, J. Y., Rodríguez, J. A., Hanson, J. C., Frenkel, A. I., Lee, P. L., 2003. Reduction of CuO and Cu_2O with H_2: H embedding and kinetic effects in the formation of suboxides. J. Am. Chem. Soc. 125, 10684 – 10692.

Guangjun. W., Naijia G., Landong L., 2011. Low temperature CO oxidation on Cu–Cu_2O/TiO_2 catalyst prepared by photodeposition. Catal. Sci. Technol. 1, 601-608.

Wan. H.Q., Wang. Z., J. Zhu, Li. X.W. Liu., B., Gao. F.,Dong. L., and Chen. Y. 2008. Influence of CO pretreatment on the activities of $CuO/\gamma\text{-}Al_2O_3$ catalysts in CO + O_2 reaction**.** Appl. Catal., B. 79, 254-261.

Choi, S.Y., Mamak, M., Coombs, N., Chopra, N., Ozin, G.A., 2004. Thermally stable two-dimensional hexagonal mesoporous nanocrystalline anatase, meso-nc-TiO_2: Bulk and crack-free thin film morphologies. Adv. Funct. Mater. 14, 335 – 344.

Sing, K.S.W., Everett, D. H., Haul, R. A. W., Moscou, L., Pierotti, R. A., Rouquérol, J., Siemieniewska, T., 1985. Reporting physisorption data for gas/solid systems with special reference to the determination of surface area and porosity (Recommendations 1984). Pure Appl. Chem. 57, 603 – 619.

Vradman, L., Landau, M.V., Kantorovich D., Koltypin, Y., Gedanken, A., 2005. Evaluation of metal oxide phase assembling mode inside the nanotubular pores of mesostructured silica. Micropor. Mesopor. Mat. 70, 307, 318.

Li, R., Weng, Y., Zhou, X., Wang, X., Mi, Y., Chong, R., Han, H., Li, C., 2015. Achieving overall water splitting using titanium dioxide-based photocatalysts of different phases. Energy Environ. Sci. 8, 2377 – 2382.

Mondal, I., Pal, U., 2016. Synthesis of MOF templated Cu/CuO@TiO_2 nanocomposites for synergistic hydrogen production. Phys. Chem. Chem. Phys. 18, 4780 – 4788.

Kandiel, T. A., Feldhoff, A., Robben, L., Dillert, R., Bahnemann, D. W., 2010. Tailored titanium dioxide nanomaterials: Anatase nanoparticles and brookite nanorods as highly active photocatalaysts. Chem. Mater. 22, 2050 – 2060.

Oros-Ruiz, S., Zanella, R., Collins, S. E., Hernández-Gordillo, A., Gómez, R., 2014. Photocatalytic hydrogen production by Au-M_xO_y (M = Ag, Cu, Ni) catalysts supported on TiO_2. Catal. Commun. 47, 1 – 6.

Yang, W. Y., Rhee, S. W., 2007. Effect of electrode on the resistance switching of Cu_2O film. Appl. Phys. Lett. 91, 232907 – 23907-3.

Saupe, G. P., Zhao, Y., Bang, J., Yesu, N. R., Carballo, G. A., Ordonez, R., Bubphamala, T., 2005. Evaluation of a new porous titanium-niobium mixed oxide for photocatalytic water decontamination. Microchem. J. 81, 156 – 162.

Hinojosa-Reyes, M., Hernández-Gordillo, A., Zanella, R., Rodríguez-González, V., 2016. Renewable hydrogen harvest process by hydrazine as scavenging electron donor using gold TiO_2 photocatalysts. Catal. Today. 266, 2 – 8.

Dholam, R., Patel, N., Adami, M., Miotello, A., 2009. Hydrogen production by photocatalytic water-splitting using Cr- or Fe-doped TiO_2 composite thing films photocatalyst. Int. J. Hydrogen Energ. 34, 5337 – 5346.

Kato, H., Kudo, A., 2002. Visible-light-response and photocatalytic activities of TiO_2 and $SrTiO_3$ photocatalysts codoped with antimony and chromium. J. Phys. Chem. B. 106, 5029 – 5034.

Khan, M. A., Woo, S. I., Yang, O. B., 2008. Hydrothermally stabilized Fe(III) doped titania active under visible light for water splitting reaction. Int. J. Hydrogen Energ. 33, 5345 – 5351.

Table 1. Percentage and crystallite size for the brookite phase in the Ti-Cu photocatalysts.

Sample	W_B[1] (%)	B/A ratio[2]	B Crystallite size (nm)
Ti-Cu 0.0	3.18	0.033	17.85
Ti-Cu 1.0	8.92	0.098	13.03
Ti-Cu 2.5	8.94	0.098	13.62
Ti-Cu 5.0	13.31	0.154	17.53
Temperature Ti-Cu 1.0	**W_B (%)**	**B/A ratio**	**B Crystallite size (nm)**
400 °C	17.55	0.213	9.46
450 °C	14.17	0.165	10.87
500 °C	8.92	0.098	13.03
550 °C	5.48	0.058	19.86
600 °C	0.00		---

[1]Brookite percentage, [2]Brookite/Anatase ratio

Table 2. Physicochemical properties of Ti-Cu photocatalysts with different copper contents, calcined at 500 °C.

	Crystallite size (nm)	Raman FWHM (cm^{-1})	Surface area ($m^2 g^{-1}$)	Cu wt. %	Eg (eV)	[1]NS_{BET}
Ti-Cu 0.0	17.7	10.4	64.6	---	3.4	---
Ti-Cu 1.0	17.5	11.7	59.5	1.0	3.3	0.93
Ti-Cu 2.5	20.0	10.8	40.0	2.5	3.2	0.63
Ti-Cu 5.0	16.2	11.0	35.2	4.6	2.3	0.57

[1]NS_{BET} (Normalized surface area) was calculate by using the equation. $NS_{BET} = (S_{BET\ of\ catalysts} / (1-x)*(S_{BET\ of\ support})$.

Table 3. Physicochemical properties of the Ti-Cu 1.0 photocatalyst calcined at different temperatures.

	Crystallite size (nm)	Raman FWHM (cm^{-1})	Surface area ($m^2 g^{-1}$)	Eg (eV)	[1]NS_{BET}
Ti-Cu 1.0 400	8.2	16.3	115.3	3.3	0.95
Ti-Cu 1.0 450	10.9	14.7	85.3	3.3	0.94
Ti-Cu 1.0 500	17.5	11.7	59.5	3.3	0.93
Ti-Cu 1.0 550	24.5	9.8	40.7	3.2	0.91
Ti-Cu 1.0 600	39.62	8.58	14.0	3.2	0.78

[1]NS_{BET} (Normalized surface area) was calculate using the equation. $NS_{BET} = (S_{BET\ of\ catalysts} /(1-x)*(S_{BET\ of\ support})$. Surface areas for Ti-400 (122 $m^2\ g^{-1}$), Ti-450 (92 $m^2\ g^{-1}$), Ti-500 (64.6 $m^2\ g^{-1}$), Ti-550 (45 $m^2\ g^{-1}$) and Ti-600 (19 $m^2\ g^{-1}$).

Table 4. Copper species ratio determinated by XPS spectroscopy.

	Cu^{1+}	Cu^{2+}	Cu^{1+}/Cu^{2+}
1.0 Cu/Ti 450	--	--	--
1.0 Cu/Ti 500	--	--	--
1.0 Cu/Ti 550	57	42	1.3
1.0 Cu/Ti 600	54	46	1.1
5.0 Cu/Ti 500	44	56	0.8

Figure captions

Figure 1. Diffractogram patterns of Ti-Cu photocatalysts with a) copper content, b) inset of the 34 – 45º region, from 0.0 to 5.0 wt. %, annealed at 500 °C, c) Ti-Cu 1.0 annealed at temperatures ranging from 400 to 600 °C, and d) inset of the 34 – 45º region

Figure 2. Raman spectra of vibrational modes of a) different copper contents annealed at 500 °C, and b) Ti-Cu 1.0 annealed at different temperatures. E_g vibrational mode of Ti-Cu photocatalysts with c) different copper contents annealed at 500 °C, and d) Ti-Cu 1.0 annealed at different temperatures.

Figure 3. XPS spectra of a) Cu2p for Ti-Cu 1.0 500, Ti-Cu 1.0 550, Ti-Cu 1.0 600, and Ti-Cu 5.0 500 photocatalysts, b) deconvolution of XPS Cu $2p^{3/2}$ core level for Cu^{1+} and Cu^{2+} in Ti-Cu 1.0 500, Ti-Cu 550, and Ti-Cu 600 photocatalysts.

Figure 4. Temperature programmed reduction of Ti-Cu photocatalysts with a) different copper loadings and b) different calcination temperatures for the Ti-Cu 1.0 sample, and its corresponding deconvoluted insets.

Figure 5. Nitrogen adsorption-desorption isotherms for the Ti-Cu photocatalysts with a) different copper loads and b) different calcination temperatures for the Ti-Cu 1.0 sample.

Figure 6. Photocatalytic hydrogen production for 8 h for the Ti-Cu samples with aa) different copper loadings, ab) induction period for these samples, ba) different annealing temperatures, bb), induction period for these samples, and c) stability test during the hydrogen photocatalytic production for Ti-Cu 1.0 annealed at 500 °C

Figure 7. Photocatalytic hydrogen production for the Ti-Cu samples with different copper loadings under visible radiation (450 nm).

Figure 8. Diffractogram patterns of Ti-Cu photocatalysts with copper contents from 0.0 to 5.0 wt. %, annealed at 500 °C, recovered after the water splitting reaction.

Figure 9. Schematic representation of the normalized surface area versus hydrogen production of a) different copper loadings annealed at 500 ºC, and b) Ti-Cu 1.0 annealed at different temperatures.

Figure 1

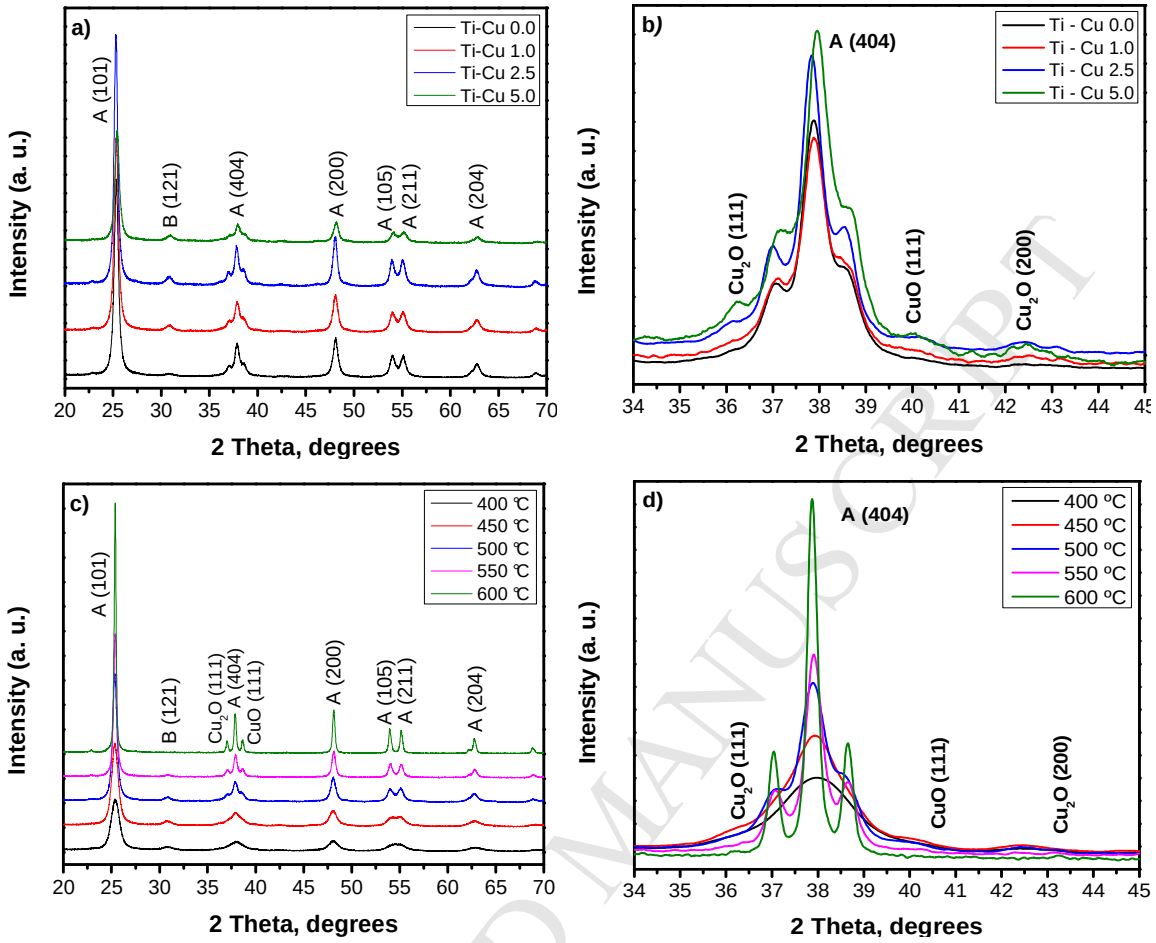

Figure 2

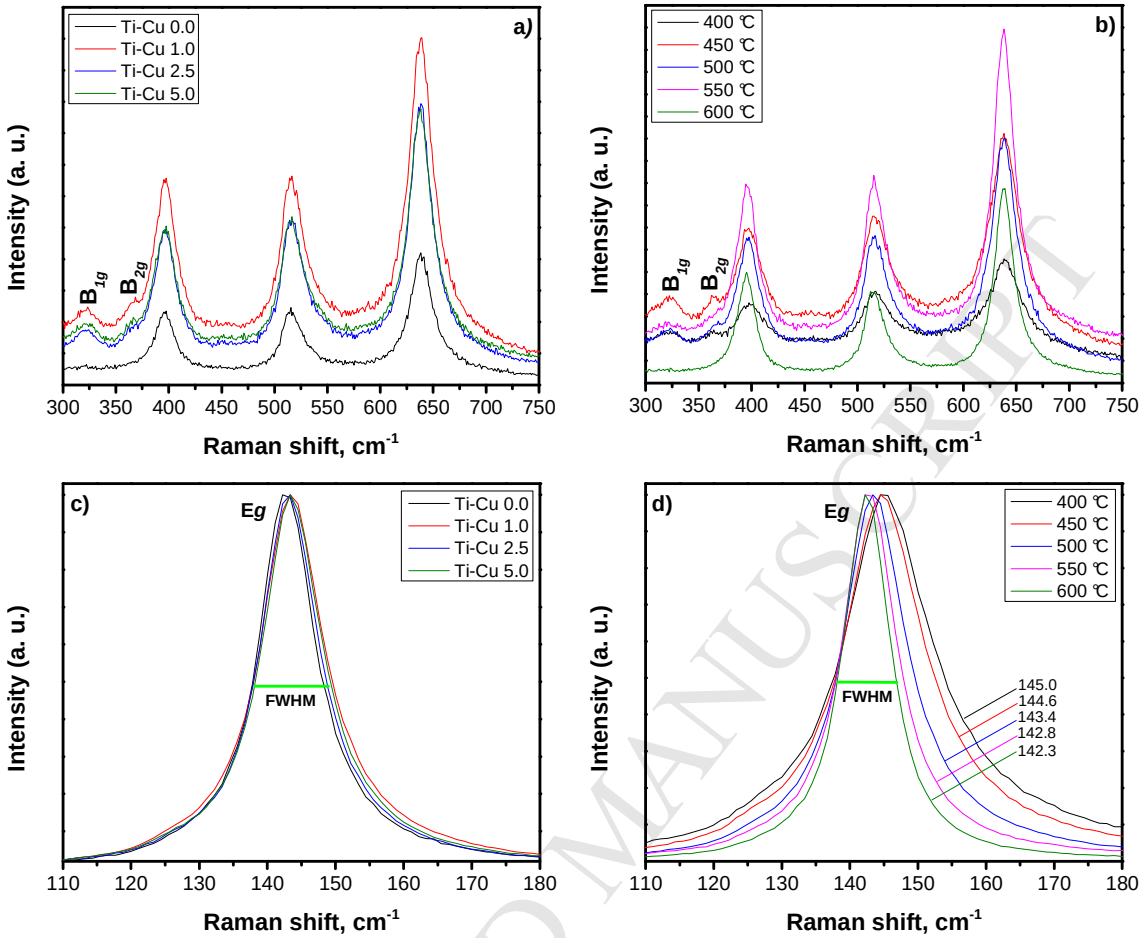

Figure 3

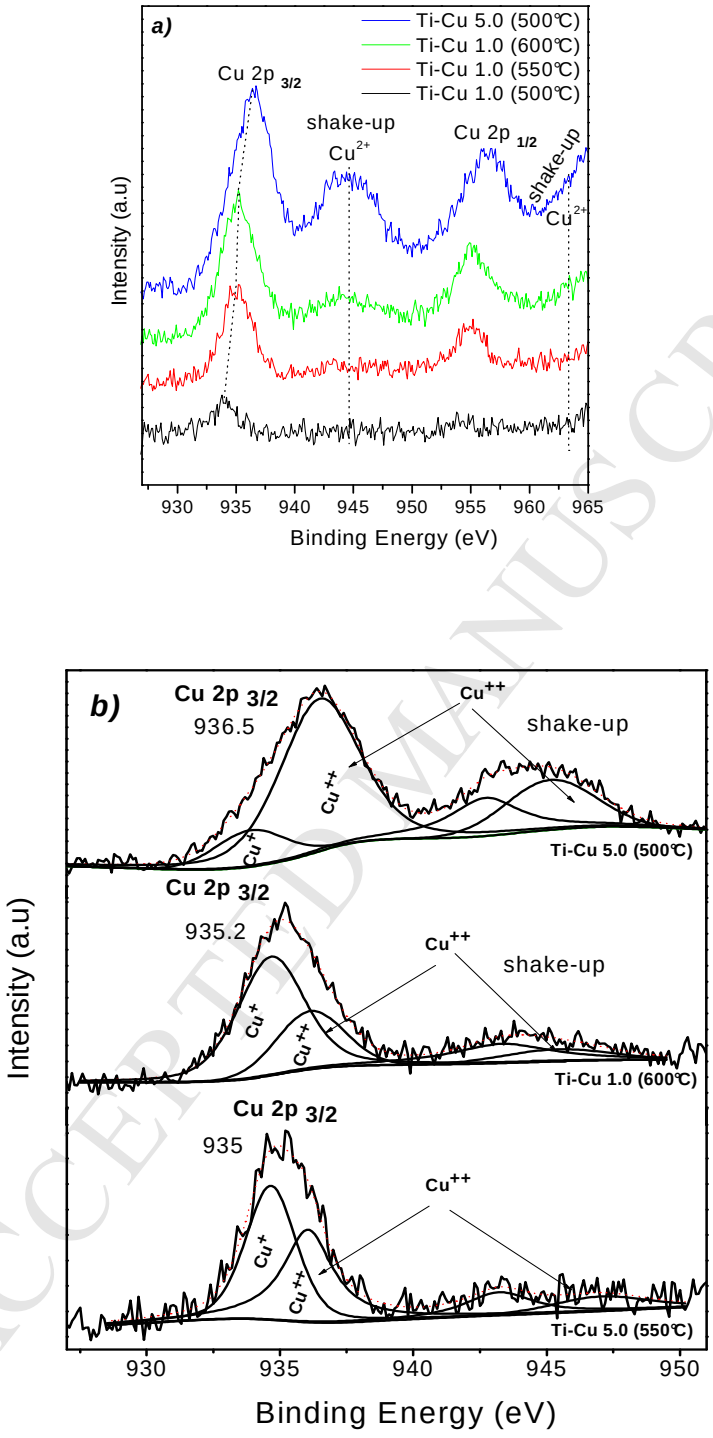

Figure 4

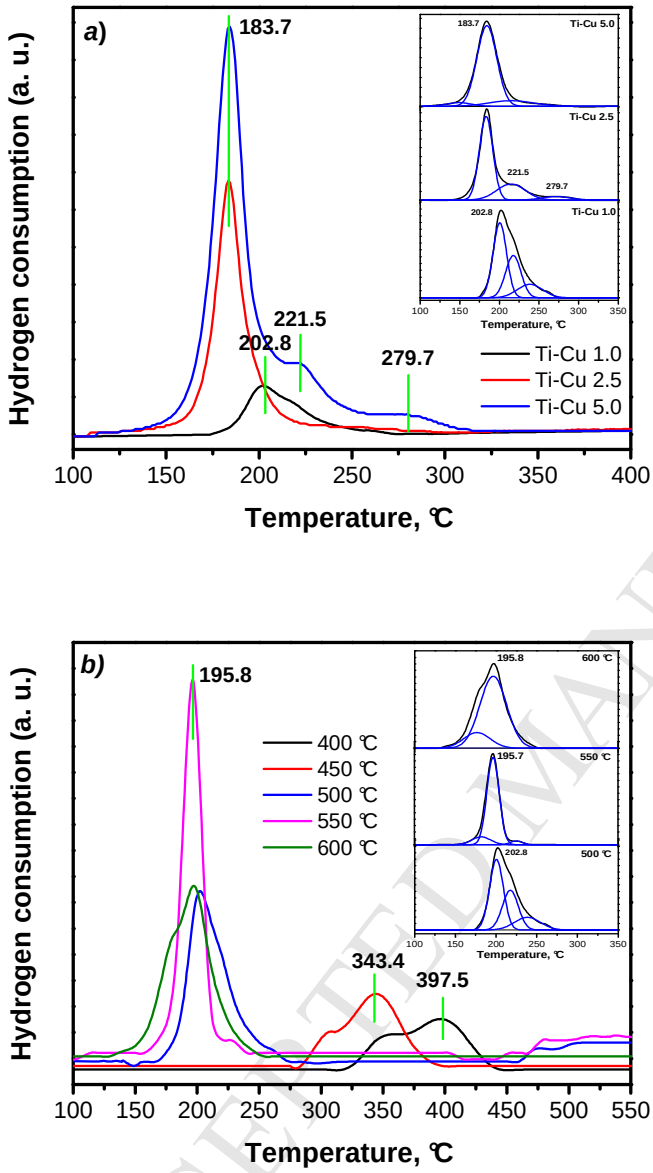

Figure 5

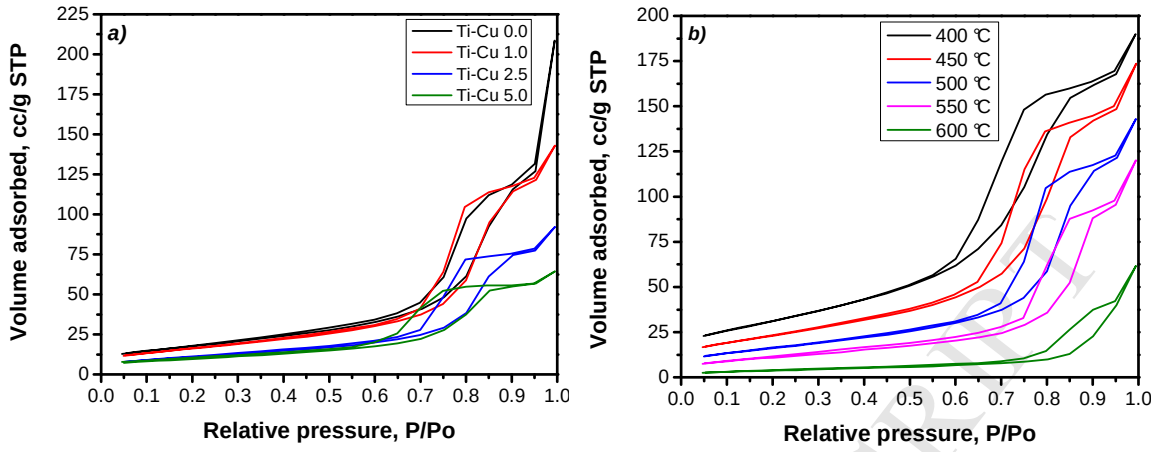

Figure 6

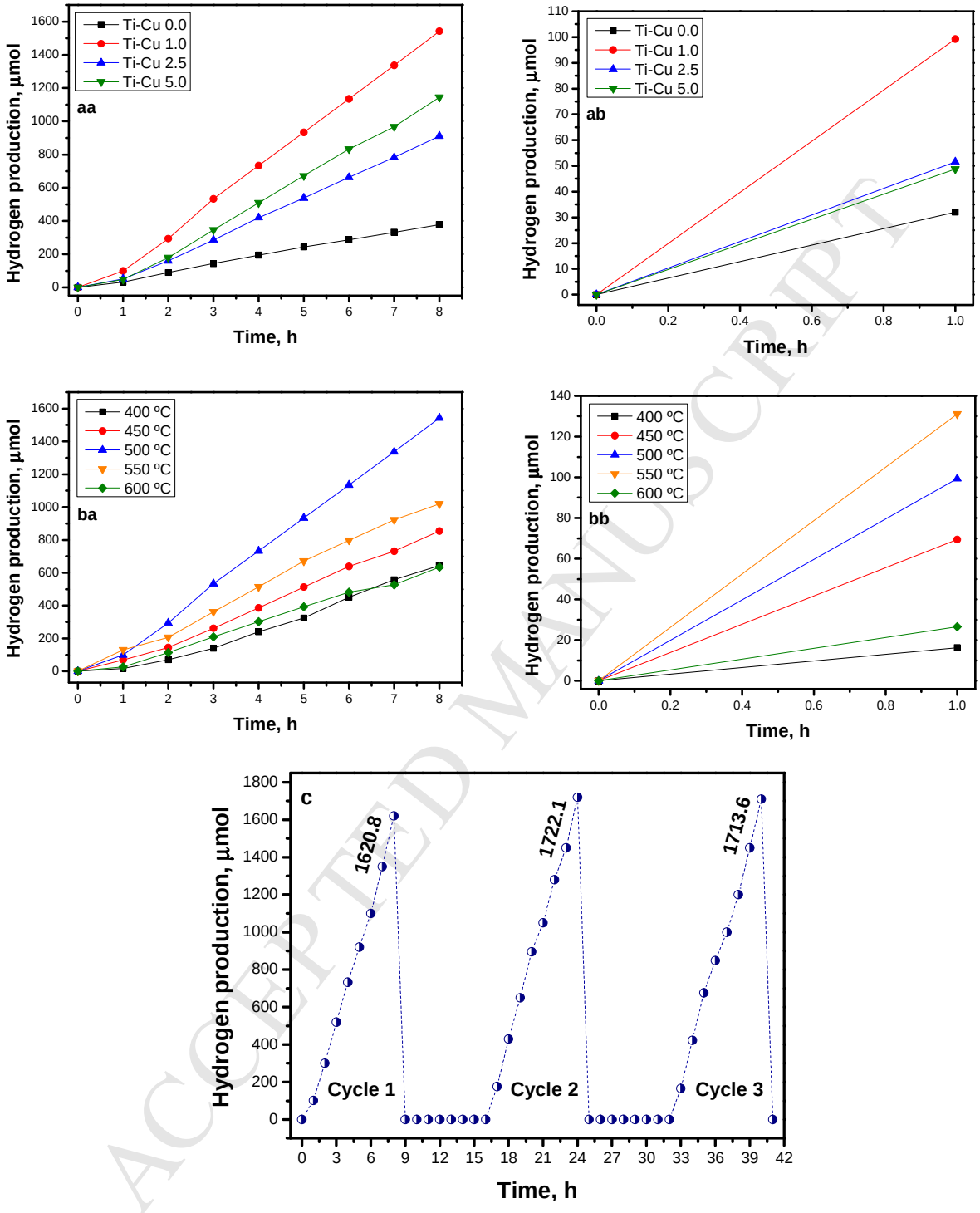

Figure 7

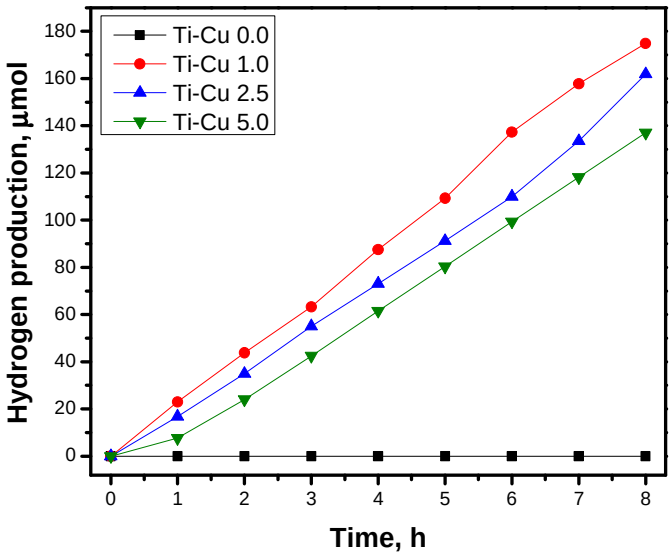

Figure 8

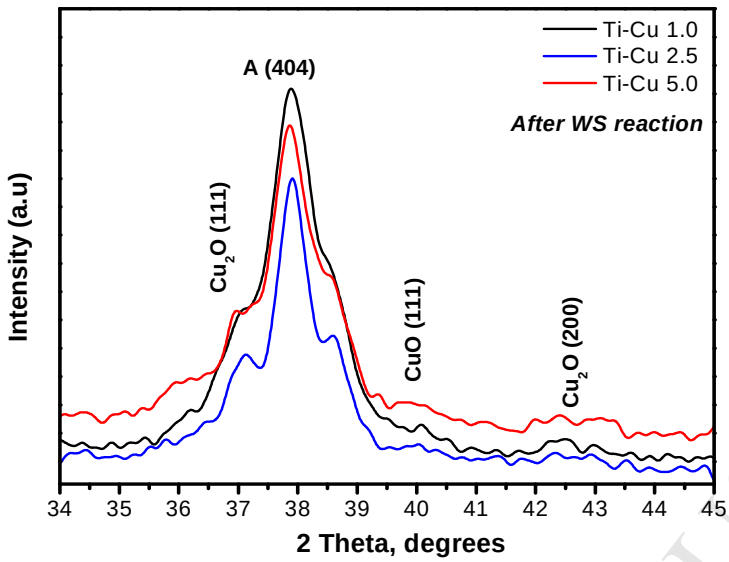

Figure 9

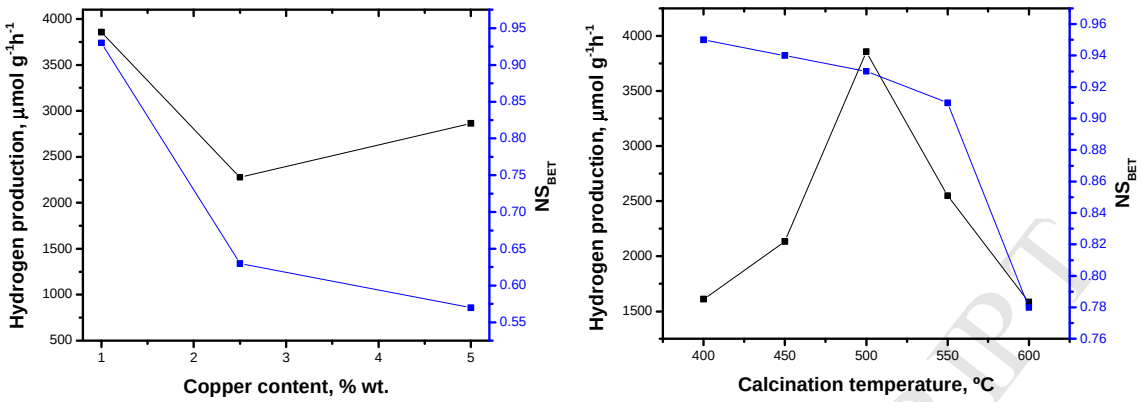

Highlights

1. The sol-gel process allows the formation of brookite and Cu_2O oxide.
2. The Ti-Cu 1.0/500 have the highest Cu^{1+}/Cu^{2+} and optimal brookite/anatase ratio.
3. Cu_2O enhances the H_2 production due to correlation between Eg and redox potentials.
4. Ti-Cu 1.0/500 photocatalyst shows the highest H_2 production without Cu lixiviation.
5. Cu catalysts represents a cost saving of 124 times in contrast with the noble metals.